Phase Diagram of Mg Insertion into Chevrel Phases, $Mg_xMo_6T_8$ (T = S, Se). 2. The Crystal Structure of Triclinic $MgMo_6Se_8$

E. Levi,*,† E. Lancry,† A. Mitelman,† D. Aurbach,† O. Isnard,‡,§ and D. Djurado||

Department of Chemistry, Bar-Ilan University, Ramat-Gan, Israel 52900, Laboratoire de Cristallographie, associé à l'Université J. Fourier CNRS, BP166X, 38042 Grenoble cédex 9, France, Institut Laue Langevin, BP 156 X, 38042 Grenoble Cedex 9, France, and Laboratoire d'Electronique Moléculaire Organique et Hybride, UMR5819-SPrAM, CEA-CNRS-Université Grenoble I, DRFMC, CEA-Grenoble, 17 rue de Martyrs, 38054 Grenoble Cedex 9, France

Received March 25, 2006. Revised Manuscript Received June 6, 2006

Chevrel phases (CPs), $M_xMo_6T_8$ (M = metal, T = S, Se), may be used as unique cathode materials for rechargeable Mg batteries because they ensure the high mobility of multivalent cations. However, the electrochemical behavior is strongly affected by the host composition. For the selenide, the intercalation process is completely reversible, while partial Mg trapping occurs upon its extraction from the sulfide at room temperature. A combination of powder X-ray and high-resolution neutron diffraction was used to study the crystal structure of triclinic $MgMo_6Se_8$, especially for determining the precise location of the Mg^{2+} cations within the host lattice. It was shown that the crystal structure of the selenide is similar to that of triclinic $Fe_2Mo_6S_8$: The Mg^{2+} cations are distributed between two sites (per formula unit) with a square-pyramidal anion coordination. The environment analysis of all the cation sites based on the bond valence sum theory led us to propose the most favorable routes for Mg^{2+} ion transport, as well as to explain the peculiarities of the electrochemical behavior of the CPs as intercalation materials for Mg batteries.

Introduction

Chevrel phases (CPs), $M_xMo_6T_8$ (M = metal, T = S, Se, Te) are of great interest owing to the variety of unusual electric, thermoelectric, magnetic, and catalytic properties.[1−4] In addition, until now this family of materials was a unique one, as it allowed the fast insertion of divalent cations.[5] The elaboration of Mg batteries based on the insertion/extraction of Mg^{2+} ions into/from electrode materials showed that both the sulfide, Mo_6S_8, and the selenide, Mo_6Se_8, can be used as cathode materials.[6−9] The insertion process occurs in two stages:

$$Mg^{2+} + 2e^- + Mo_6T_8 \leftrightarrow MgMo_6T_8 \quad (1)$$

$$Mg^{2+} + 2e^- + MgMo_6T_8 \leftrightarrow Mg_2Mo_6T_8 \quad (2)$$

However, the electrochemical behaviors of these two hosts are essentially different. For the selenide, the process is completely reversible, while Mg trapping occurs upon its extraction from the sulfide at room temperature. (Full Mg extraction in the latter case is possible only at elevated temperatures). Moreover, the kinetics of Mg insertion into Mo_6Se_8 is faster than that into Mo_6S_8. It was suggested[9] that this effect originated from the higher polarizability of the selenium anionic framework, as compared to the sulfur one. Nevertheless, it remained difficult to fully understand the influence of the anionic framework on the cation mobility without detailed knowledge of the crystal structure of the corresponding intercalation compounds.

In general, to understand the mechanism of ionic motion in solids, we should know not only the arrangement of the sites in the crystal structure, which can be occupied by cations, but also that of the transport sites.[10] The latter have a higher energy of the site's occupation than the former one, and so normally they are empty. However, the transport sites play an important role in ion migration by essentially decreasing the activation energy of the ion hopping. Thus, to elucidate the peculiarities of the cation mobility in CPs with different compositions, we have to follow the pathway of the inserted cations through their crystal structure. For this it is first necessary to determine the precise crystal structure of the Mg intercalation compounds and, subsequently, to analyze the distribution of all the possible cation sites (including the transport ones). Hence, the previous part of this work was devoted to studying the $Mg_xMo_6S_8$ ($x = 1$

† Bar-Ilan University.
‡ associé à l'Université J. Fourier CNRS.
§ Institut Laue Langevin.
|| CEA-CNRS-Université Grenoble I.

(1) *Topics in Current Physics: Superconductivity in Ternary Compounds I*; Fisher. Ø., Maple, M. B., Eds.; Springer-Verlag: Berlin, 1982.
(2) Yvon, K. In *Current Topics in Material Science*; Kaldis, E., Ed.; Elsevier: North-Holland, Amsterdam, 1979; Vol. 3.
(3) Nunes, R. W.; Mazin, I. I.; Sigh, D. *J. Phys. Rev. B* **1999**, *59*, 7969.
(4) Benson, J. W.; Schrader, G. L.; Angelici, R. J. *J. Mol. Catal. A* **1995**, *96*, 283.
(5) Schollhorn, R. *Angew. Chem., Int. Ed. Engl.* **1980**, *19*, 983.
(6) Aurbach, D.; Lu, Z.; Schechter, A.; Gofer, Y.; Gizbar, H.; Turgeman, R.; Cohen, Y.; Moskovich, M.; Levi, E. *Nature* **2000**, *407*, 724.
(7) Aurbach, D.; Gofer, Y.; Lu, Z.; Schechter, A.; Chusid, O.; Gizbar, H.; Cohen, Y.; Ashkenazi, V.; Moskovich, M.; Turgeman, R.; Levi, E. *J. Power Sources* **2001**, *97*, 28.
(8) Aurbach, D.; Weissman, I.; Gofer, Y.; Levi, E. *Chem. Rec.* **2003**, *3*, 61.
(9) Levi, M. D.; Lancry, E.; Levi, E.; Gizbar, H.; Gofer, Y.; Aurbach, D. *Solid-State Ionics* **2005**, *176*, 1695.
(10) West, A. R. *Basic Solid State Chemistry*; John Wiley & Sons: Chichester, 1988.

10.1021/cm060715m CCC: $33.50
Published on Web 07/11/2006

and 2) crystal structures.[11] It was shown that the latter is similar to the crystal structure of rhombohedral $Cu_xMo_6S_8$. In this paper, we present the results related to $MgMo_6Se_8$, as well as a comparative analysis of the Mg transport routes for the sulfides and selenides.

In the classic review by Fischer et al.,[1] the Mg-containing selenides, $Mg_xMo_6Se_8$, were mentioned as triclinic phases, but other additional information was not presented. In general, the transformation from rhombohedral (R) to triclinic (T) symmetry is a well-known phenomenon for CPs.[1,2] For instance, at room temperature, cations in $Cu_2Mo_6S_8$ are distributed statistically between six equivalent tetrahedral positions linked to each other by a -3 symmetric axis. Hence, the symmetry of the crystal structure is rhombohedral. At a low temperature, only two of the six tetrahedra are occupied by cations. In the latter case, dumbbells are used to describe the identical cation positions connected to each other by the inversion center -1. As a result, the symmetry of the phase is triclinic. The R $\rightarrow$ T phase transition usually occurs upon cooling, and thus it was interpreted as the "freezing" of the previously mobile cations in the fixed positions in the crystal structure.[12]

The relationship between the symmetry and the composition for CPs is more complicated. Earlier studies[1,2] correlated the symmetry of $M_xMo_6T_8$ (M = small cations) at room temperature to the metal content x. Moreover, in a classic review,[1,2] the CPs were classified according to their symmetry: (i) phases that maintain the same symmetry in the full range of x and (ii) phases that change the symmetry from R to T at a higher M content. However, it was later shown that some of the CPs, which were initially identified as T phases, are actually of the R symmetry. (For instance, compare the results of refs 13 and 14 with those of refs 15 and 16 for $Li_xMo_6T_8$ (T = S, Se), those of ref 1 with those of ref 17 for $M_xMo_6T_8$ (M = Zn, Cd; T = S, Se), or those of refs 1 and 2 with those of ref 11 for $Mg_xMo_6S_8$.)

The reason for such confusion in some cases may be related to the high atmospheric instability of most of the metal-rich CPs, which lose the metal in the presence of any oxidizing agent.[11,18] Subsequently, the material might present a mixture of two or even three phases with close unit-cell parameters, which may be confused in the phase analysis with a single T phase. The wrong interpretation might be more probable for the CPs with a high metal concentration, because the susceptibility for atmospheric oxidation increases with the metal amount in CPs. Thus, any information about triclinic symmetry for CPs should be carefully verified.

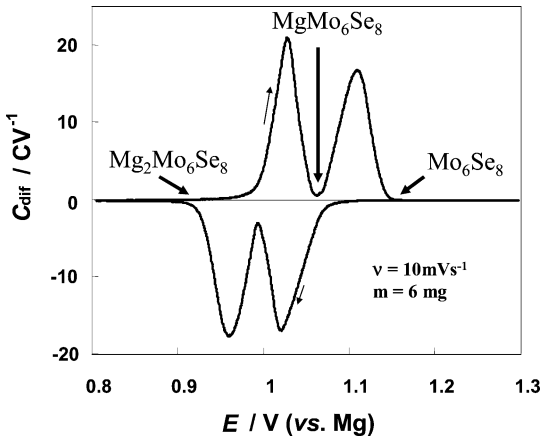

Figure 1. Slow scan cyclic voltammetry curve (plot of current I vs potential E, presented in the form of the differential capacitance, $C_{dif} = I/\nu$, where ν is the potential scan rate, equal to 10 μV/s) for the Mg^{2+} ion insertion into Mo_6Se_8. Redox peaks correspond to the phase transitions described in the reactions 1 and 2.

According to recent data,[11,13,14,17] the case of the R $\rightarrow$ T transition, associated with the increase in the metal content, is not so common at room temperature as was stated in the earlier reviews, although such a transition is well-established for iron sulfides.[1] However, an opposite example is presented by the selenides of Ni with T symmetry for low Ni concentration ($x = 0.66$)[19] and the R one for $x = 1.2$.[20] In addition, the symmetry of the CPs depends on the character of the anion framework: The T symmetry is more common for the selenides than for the sulfides, especially for the selenides of transition metals.[21] The freezing mechanism is not suitable for explaining the R $\rightarrow$ T phase transition in the latter case[21] because it disagrees with the well-known higher mobility of cations in selenides, as compared to sulfides.[10]

Thus, the aim of this paper was to resolve the crystal structure of the Mg-containing selenides, to determine all possible cation sites (including the transport ones) and to clarify their relation to the symmetry, as well as to explain the distinctive differences of the cation mobility in the sulfides as compared with the selenides.

Experimental Section

The process for electrochemical Mg insertion into Mo_6Se_8 was described earlier.[9] The host, Mo_6Se_8, was synthesized by the reaction of the powder element mixture in an evacuated (10^{-3} Torr) sealed quartz tube (170 h at 1200 °C, followed by quenching in an ice/water bath). As can be seen from Figure 1, the compounds with stoichiometry $MgMo_6Se_8$ and $Mg_2Mo_6Se_8$ can be obtained at potentials of 1.035 and 0.9 V versus magnesium, respectively.

The product of chemical Mg insertion, $Mg_2Mo_6Se_8$, was obtained via the topotactic reaction of the binary Mo_6Se_8 in contact with a Ph_2Mg/tetrahydrofuran (THF) solution as the source of Mg ions and as the reducing agent. Ph_2Mg was synthesized from PhMgCl (Aldrich) according to the Schlenk equilibrium:

(11) Levi, E.; Lancry, E.; Mitelman, A.; Aurbach, D.; Ceder, G.; Morgan, D.; Isnard, O. Phase Diagram of Mg Insertion into Chevrel Phases, $Mg_XMo_6T_8$ (T = S, Se). 1. Crystal Structure of the Sulfides. *Chem. Mater.*, to be submitted.
(12) Yvon, K.; Baillif, R.; Flukiger, R. *Acta Crystallogr.* **1979**, *B35*, 2859.
(13) Ritter, C.; Gocke, E.; Fischer, C.; Schollhorn, R. *J. Mater. Res. Bull.* **1992**, *27*, 1217.
(14) Gocke, E.; Schollhorn, R.; Aselmann, G.; Muller-Warmuth, W. *Inorg. Chem.* **1987**, *26*, 1805.
(15) McKinnon, W. R.; Dahn, J. R. *Phys. Rev. B: Condens. Matter* **1985**, *31*, 3084.
(16) Dahn, J. R.; McKinnon, W. R.; Coleman, S. T. *Phys. Rev. B: Condens. Matter* **1985**, *31*, 484.
(17) Gocke, E.; Schramm, W.; Dolscheid, P.; Schollhorn, R. *Solid State Chem.* **1987**, *70*, 71.
(18) Tarascon, J. M.; Disalvo, F. J.; Murphy, D. W.; Hull, G. W.; Rietman, E. A.; Waszczak, J. V. *Solid State Chem.* **1984**, *54*, 204.
(19) Bars, O.; Guillevic, J.; Grandjen, D. J. *Solid State Chem.* **1973**, *6*, 335.
(20) Belin, S.; Chevrel, R.; Sergent, M. J. *Solid State Chem.* **2000**, *155*, 250.
(21) Mancour-Billah, A.; Chevrel, R. J. *Solid State Chem.* **2003**, *170*, 281.

$$2RMgX \rightarrow R_2Mg + MgX_2.$$

1,4-Dioxane was used to shift the equilibrium to the right.

The product of solid-state synthesis, $MgMo_6Se_8$, was prepared at a relatively low temperature (650 °C) by heating Mg powder and the binary Mo_6Se_8 in an evacuated, sealed quartz tube for a week. To prevent the Mg to react with the quartz, a corundum crucible inside the tube was used. To ensure the desirable stoichiometry of the product after its air stabilization (see Results and Discussion), the Mg concentration in the initial mixture was 1.5 times higher than that in the intended formula, $MgMo_6Se_8$.

X-ray diffraction (XRD) studies were performed with a Bruker, Inc. (Germany), AXS D8 ADVANCE diffractometer (reflection $\theta-\theta$ geometry, Cu Kα radiation, receiving slit 0.2 mm, scintillation counter). Mylar film was used to prevent oxygen access to the samples that were sealed for XRD analysis in an Ar-containing glovebox. Diffraction data for the Rietveld refinement were collected with a Gobel mirror (parallel beam) in the angular range of $10° < 2\theta < 110-140°$, step size 0.02°, step time 10 s/step. The experiments at elevated temperatures were carried out in an evacuated camera HTK 16 on a Pt heating filament.

The neutron diffraction experiments were performed at the Institut Laue Langevin at Grenoble, France, on a D1A instrument. A detailed description of this instrument is available via the Internet at http://www.ill.fr. D1A is a very high-resolution powder diffractometer operating with the takeoff angle of the monochromator at 122°. In the configuration used, the resolution of D1A was about 0.3° (full width at half-maximum) at 90°. The measurements were carried out at a wavelength of $\lambda = 1.911$ Å selected by the (115) reflection of a germanium monochromator. During the neutron diffraction measurements a cylindrical vanadium sample holder of 7 mm inner diameter was used. The neutron detection was performed with a set of 6° spaced ^{3}He counting tubes. The complete diffraction pattern was obtained by scanning over the whole 2θ range.

The data were analyzed by the Rietveld structure refinement program FULLPROF.[22] Agreement factors used in this article are defined according to the guidelines of the Rietveld refinement that can be found elsewhere.[23] The neutron scattering lengths used were $b_{Se} = 0.7970 \times 10^{-14}$ m, $b_{Mg} = 0.5375 \times 10^{-14}$ m, *and* $b_{Mo} = 0.6715 \times 10^{-14}$ m, values taken from ref 24.

Results and Discussion

Preliminary Material Characterization. As can be seen from the experimental section, three different methods were used to obtain the CPs: (i) direct HT synthesis (or thermal intercalation) and (ii) chemical and (iii) electrochemical cation insertion into the host, Mo_6Se_8. In general, the electrochemical and chemical insertions in the host without impurities give the purest products, but in the case of Mo_6Se_8 such products are extremely unstable under air. In addition, the electrodes containing supplementary components, such as stainless steel backing, carbon black, and poly(vinylidene difluoride) binder, are less suitable for the Rietveld refinement, especially in the case of the triclinic phases.

As mentioned previously, the solid-state synthesis can give an air stable powder only after surface oxidation by exposure to air, and the formation of protecting compact MgO surface films around the CPs' particles. Spontaneous, rapid Mg extraction yields the stabilization layer. Thus, the synthetic product with a stoichiometry of $MgMo_6Se_8$ can be obtained only when an excess of Mg is used for the initial synthesis mixture. The latter material is the most convenient for structural analysis, although it usually contains some impurities. In contrast, it is impossible to use the same strategy to stabilize the compound with a $Mg_2Mo_6Se_8$ stoichiometry, because the initial Mg content in the crystal structure cannot exceed two Mg atoms per formula unit. Hence, in this case the most convenient method for the material preparation for structural analysis is chemical insertion, while the samples under study should be kept under highly inert atmosphere during the experiment. Until now, our attempts to prepare the Mg-rich selenide for neutron diffraction studies were unsuccessful because of its high instability.

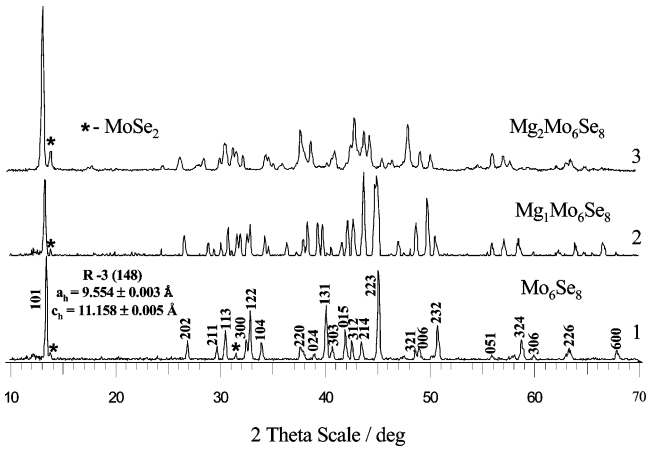

Figure 2. XRD patterns of $Mg_xMo_6Se_8$ obtained at different stages of the electrochemical intercalation (three different electrodes): $1 - x = 0$; $2 - x = 1$, and $3 - x = 2$.

Figure 2 presents the XRD patterns of $Mg_xMo_6Se_8$ ($x = 0$, 1, and 2), obtained at different stages of the electrochemical intercalation (three different electrodes). The host pattern ($x = 0$) is identical to JCPDS-ICDD, 24-0772: space group $R\bar{3}$ (No. 148), $a_h = 9.57$ Å, and $c_h = 11.15$ Å. In contrast, the patterns for $x = 1$ and 2 cannot be indexed as rhombohedral phases or their mixtures, supporting the suggestion that Mg insertion into Mo_6Se_8 results in the triclinic distortion of the crystal structure.

In Figure 3a,b, the XRD patterns of $Mg_xMo_6Se_8$ ($x = 1$ and 2), obtained by different synthetic routes, are compared. Aside from the presence of some additional peaks, related to various impurities, any difference in the XRD patterns was not assigned for the intercalation products with a different history. Similar results were previously obtained for other CPs.[11,13,14]

As discussed in the introduction section, CP heating should result in the transformation of the triclinic structure to the rhombohedral one. This phase transition, occurring upon heating, was used to substantiate the triclinic distortion in the material under study, as well as to estimate the average unit cell parameters for the T form (the latter are usually close to the unit cell parameters of the R form). Figure 4 compares the XRD patterns of $MgMo_6Se_8$ obtained at room temperature and 300 °C. As can be seen, phase transition

(22) Carjaval, J. R. *Physica B* **1993**, *192*, 55.
(23) McCusker, L. B.; Von Dreele, R. B.; Cox, D. E.; Louer, D.; Scardi, P.*J. Appl. Crystallogr.* **1999**, *32*, 36.
(24) Sears, V. F. *Neutron News* **1992**, *3*, 26.

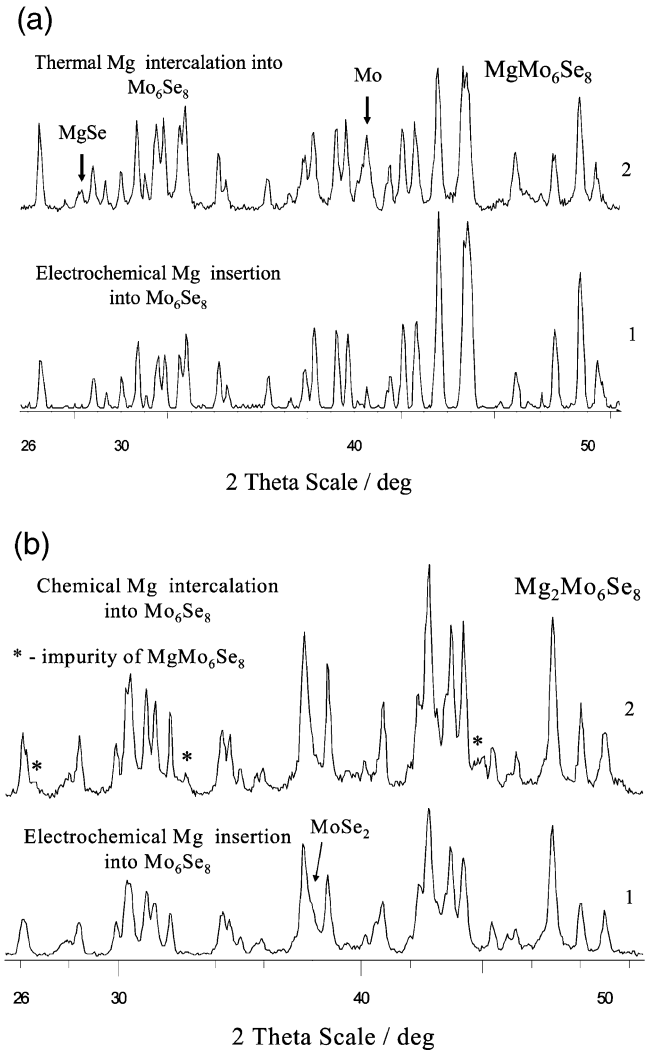

Figure 3. XRD patterns of $Mg_xMo_6Se_8$ obtained by different synthetic routes. (a) $x = 1$: 1, Electrochemical Mg insertion into Mo_6Se_8; 2, thermal Mg intercalation into Mo_6Se_8. (b) $x = 2$: 1, Electrochemical Mg insertion into Mo_6Se_8; 2, chemical Mg intercalation into Mo_6Se_8.

clearly occurs, and this process is fully reversible: the XRD pattern obtained after cooling is identical to the initial one.

As expected, the unit cell parameter of the R cell for the high-temperature form, $a_r = 6.75 \pm 0.02$ Å, is close to that of the other selenides. For instance, a_r for $Cu_xMo_6Se_8$ changes from 6.71 Å for $x = 1$ to 6.78 Å for $x = 2$.[1,2] Another important parameter obtained in this experiment is the value of the rhombohedral angle α. As is known,[1,2] this angle correlates with the cation delocalization from the cavity's center. For $MgMo_6Se_8$, the angle, equal to $93.1 \pm 0.2°$, is lower than that for $Cu_xMo_6Se_8$ (93.8 for $x = 1$ and 94.7 for $x = 2$).[1,2] It can be suggested that a strong repulsion between the divalent Mg^{2+} cation and molybdenum results in a smaller cation delocalization than that in the case of monovalent cations. Similar results were obtained for the sulfides.[11]

Rietveld Refinement. The unit cell parameters of the R form, obtained in the experiment at elevated temperature, were used as the initial ones for the Rietveld refinement of the triclinic phase. Concerning the other parameters of the initial model, it was shown previously[1,2,21,25] that the positions of the host (Mo and S/Se) atoms in the crystal structure are almost constant for different compositions, temperatures, or even symmetries of the CPs. As a result, the positions of the sites available for cation insertion are also very similar for different CPs, despite the variation in the site's occupation.

According to the latter parameter, the CPs with small cations can be divided into two major groups. In the first group the cations occupy preferentially cavity 1, while in the second they are located only in cavity 2. Moreover, the cation positions in cavity 2 for the two groups are different. As a result, the cations in the second group are located essentially closer to the Mo atoms; thereby, this group is typical for the selenides of the transition metals with specific metal−metal interactions. For instance, the M−Mo distance for $CuMo_6Se_8$ (first group CP) is equal to 3.53 Å (for the Cu^+ in cavity 1),[2] while the same distance for the second group changes from 2.79 Å for $Ti_{0.88}Mo_6Se_8$ to 2.48 Å for $Ni_{1.25}Mo_6Se_8$ (the cations are in "new positions" in cavity 2).[25] It seems evident that $MgMo_6Se_8$ should be related to the first group because of the strong polarizing character of the Mg^{2+} ions. Thus, the atomic positions of the rhombohedral $CuMo_6Se_8$ were taken as the initial ones in the Rietveld refinement of the triclinic $MgMo_6Se_8$.

Figure 5a,b presents the neutron Rietveld profiles for $MgMo_6Se_8$ obtained by two synthetic routes, thermal and chemical Mg insertion, respectively. Initially the neutron profiles for these materials were refined separately, but owing to the very similar results, at the last stage of the refinement they were combined (multi-pattern refinement). In the case of chemical intercalation, the aim was to obtain the compound with $Mg_2Mo_6Se_8$ stoichiometry. However, the attempt was unsuccessful, and the $Mg_2Mo_6Se_8$ decomposition resulted in a mixture of $MgMo_6Se_8$ and Mo_6Se_8.

It should be noted that the Mg extraction from the CPs' crystal structure, due to the material oxidation in the case of the thermal intercalation, is confirmed by the presence of a small amount of MgO in the sample under study. In contrast, in the case of chemical Mg insertion, any additional Mg-containing phase that should result from the material decomposition was not discovered. However, we have to take into account that the amount of Mg, which was extracted from the crystal structure of the CPs during the decomposition, did not exceed ~1 wt %. In addition, such a phase might be amorphous or dissolve during rinsing in THF. Thus, its identification in the diffraction analysis might be impossible.

The atomic thermal parameters (0.33 $Å^2$ for Mo, 0.5 $Å^2$ for Se, and 1 $Å^2$ for Mg) used in the calculation model were chosen according to the literature data[21] and kept constant. The occupation numbers were not refined; they corresponded to the $MgMo_6Se_8$ stoichiometry verified previously by inductively coupled plasma analysis and electrochemical titration. The refinement of the peak shape and asymmetric parameters showed that their values for all the phases were similar or close to that of the standards (well-crystallized cubic materials) measured under the same experimental conditions. Thus, the samples under study are also well-crystallized.

(25) Roche, C.; Chevrel, R.; Jenny, A.; Pecheur, P.; Scherrer, H.; Scherrer, S. *Phys. Rev. B* **1999**, *60*, 16442.

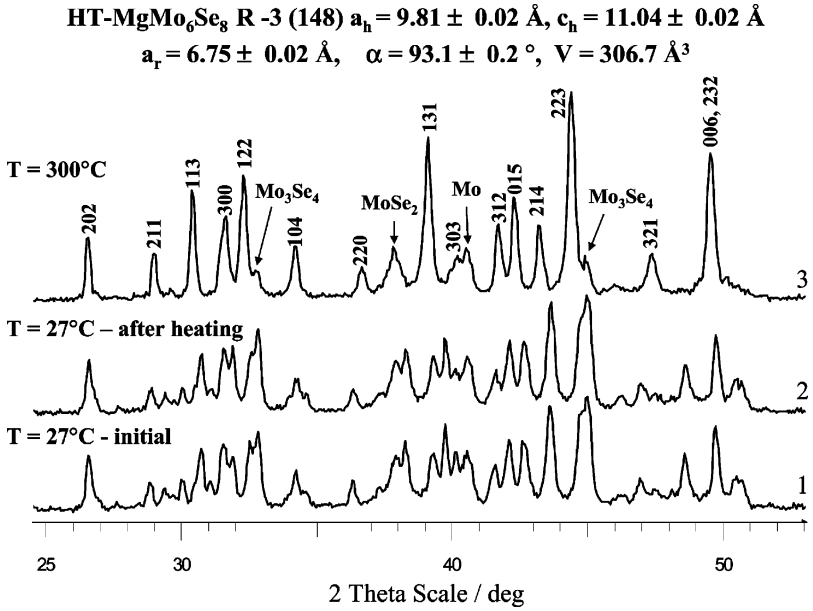

Figure 4. XRD patterns of $Mg_XMo_6Se_8$ obtained at different temperatures: 1, initial material at room temperature; 2, the same material after heating; and 3, the same material at 300 °C.

Table 1 presents the atomic positions and their standard deviations (in parentheses) for the crystal structure of $MgMo_6Se_8$. Mg^{2+} ions occupy the so-called "inner sites" located in cavity 1. Their positions are close to that described in the literature.[1,2] The calculations show that the probability for the outer site's occupation in cavity 2 is very low (within the limits of the calculation accuracy). In the case where the initial model was similar to that of the Chevrel selenides containing transition metals[21] (alternative positions in cavity 2), the R factors were essentially higher, while the refinement of the Mg atomic coordinates resulted in their shift to the outer sites. Thus, the initial model for the Rietveld analysis is correct, and the crystal structure of $MgMo_6Se_8$ is basically similar to that of the Cu-containing selenides, despite the difference in their symmetry. To confirm the refined crystal structure, the results of the neutron diffraction were verified by fitting the XRD pattern using the same model (Figure 6).

The atomic positions presented in Table 1 were used to calculate the interatomic distances and their standard deviations (Table 2). As can be seen, the values, obtained by the refinement, are consistent. They confirm the stability of the rigid structure for the Mo_6Se_8 cluster, despite the additional degree of freedom in the atomic coordinates caused by the triclinic distortion. For comparison, Table 2 also contains the interatomic distances in the crystal structure of $Cu_2Mo_6Se_8$. The latter values were calculated according to the atomic positions presented in the literature.[1]

This comparison demonstrates not only the similarity between the crystal structures of the Mg- and Cu-containing selenides but also their differences. First of all, the delocalization of the Mg^{2+} ions from the center of cavity 1 is clearly smaller than that of the Cu^+ ions. (Compare the Mg−Mg and Cu−Cu distances in Table 2 that are equal to ∼1.93 and 2.24 Å, respectively. Note once again that we are not speaking here about the distance between two cations but rather about that between two cation sites that cannot be occupied simultaneously.) As was mentioned previously, the same phenomenon was found for the high-temperature rhombohedral form, as well as for the corresponding sulfides.[11] We believe that it is caused by the higher repulsion between Mo and divalent Mg^{2+} ions, as compared to the monovalent Cu^+ cations. In fact, the Mo−Mg distance is clearly longer than that of Mo−Cu (∼3.7 and 3.5 Å, respectively).

In addition, there is an obvious difference in the Mg and Cu coordination by selenium atoms. It is clear that the coordination number (CN) of Cu in the CP selenide is 4, because the four Cu−Se distances are very close (∼2.5 Å), while the fifth one is much longer (∼3.5 Å). In contrast, for $MgMo_6Se_8$, all five of the Mg−Se distances do not differ essentially from the sum of the ionic radii of Mg^{2+} (0.74 Å) and Se^{2-} (1.93 Å), equal to 2.67 Å. (Here the ionic radii are given for CN = 6). In fact, the difference does not exceed 10%, and thereby it is logical to suggest that the CN of Mg is 5. Hence, the crystal structure of $MgMo_6Se_8$ is similar to that of triclinic $Fe_2Mo_6S_8$.[1] In both compounds, the cations are located at the center of the square pyramids formed by anions of cavity 1.

The crystal structure solution can be confirmed by the calculation of the bond valence sum (BVS) for the Mg^{2+} cation (Table 2). According to the bond valence (BV) theory,[26,27] based on the Pauling second rule of the local electroneutrality, there is an exponential dependence between the length of the bonds around any atom in the crystal structure of the ionic compound and the BV:

$$s_{ij} = \exp[(R_1 - R_{ij})/b] \qquad (3)$$

where R_{ij} is the distance between atom i and its neighbor j, s_{ij} is the BV or the electrostatic bond strength, and R_1 and b are the empirical constants with $b = 0.37$ Å, while R_1 is a tabulated parameter for each cation−anion pair. For instance,

(26) Brese, N. E.; O'Keefee, M. *Acta Crystallogr.* **1991**, *B47*, 192.
(27) Brown, I. D. *Acta Crystallogr.* **1992**, *B48*, 553.

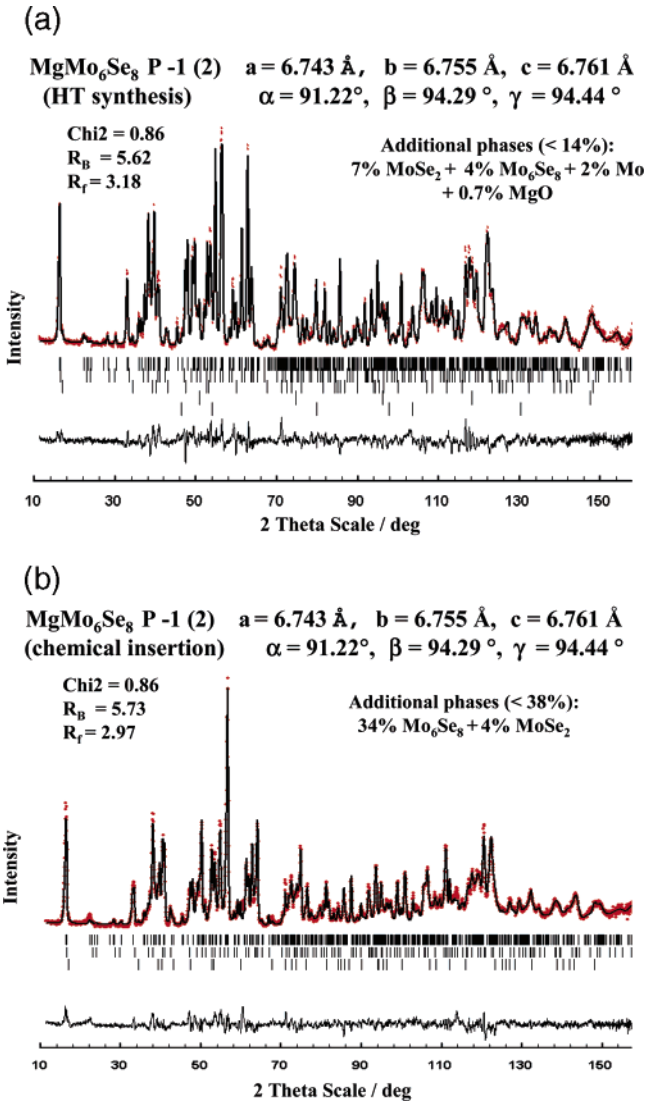

Figure 5. Neutron Rietveld profiles for $MgMo_6Se_8$: (a) product of thermal Mg intercalation into Mo_6Se_8; (b) product of chemical Mg insertion into Mo_6Se_8.

Table 1. Atomic Coordinates for the Crystal Structures of $MgMo_6Se_8$[a]

atom	site	*X*	*Y*	*Z*	occ.
Mo1	2i	0.2396(15)	0.4069(14)	0.5364(14)	1
Mo2	2i	0.4112(14)	0.5496(14)	0.2357(14)	1
Mo3	2i	0.5450(14)	0.2239(13)	0.4166(13)	1
Se_1	2i	0.1255(13)	0.7344(11)	0.3749(12)	1
Se_2	2i	0.3659(11)	0.1215(11)	0.7456(12)	1
Se_3	2i	0.7335(12)	0.3884(11)	0.1401(10)	1
Se_4	2i	0.2087(10)	0.2237(11)	0.2113(11)	1
Mg	2i	0.116(3)	0.925(3)	0.999(3)	0.5

[a] $MgMo_6Se_8$ $P\bar{1}$ (No. 2), $a = 6.743$ Å, $b = 6.755$ Å, $c = 6.761$ Å, $\alpha = 91.22°$, $\beta = 94.29°$, and $\gamma = 94.44°$.

for the Mg−Se pair, $R_1 = 2.32$ Å.[26] The BVS is equal to the total atom valence *V*:

$$\sum s_{ij} = V \tag{4}$$

Thus, if the crystal structure determination is correct, the BVS of any atom calculated according to the experimental interatomic distances should be equal to the expected value of its oxidation state. It is clear that this value for the Mg^{2+} cation should be close to 2. The results of such simple calculations (Table 2) show that the BVS for the Mg^{2+} cation is equal to 2.07, confirming, in general, the crystal structure suggested and, in particular, the CN = 5.

At first glance, the change from the tetrahedral anion configuration around Mg in the sulfides, $Mg_xMo_6S_8$ ($x = 1$ and 2),[11] to the square pyramid in the selenide seems surprising. According to Pauling's first rule, an increase in the anion size might only decrease the cation CN. To explain this unusual change, let us verify which CN is predicted for the Mg^{2+} ion by the BV theory. In stable compounds, the CN of all atoms should be close to the characteristic one, which can be found by the equation[27]

$$\langle CN \rangle = V/S_a \tag{5}$$

where V is the cation valence (formal oxidation state) and S_a is the Lewis acid strength.

For the Mg^{2+} cation, $V = 2$ and $S_a = 0.334$. Thus, the characteristic CN of the Mg^{2+} ions in crystal structures should be equal to 6. In fact, this CN is realized, for instance, in MgS and MgSe with the NaCl-type crystal structure. Hence, the increase of the CN up to 5 found in the selenide should be related to the stabilization of the crystal structure. In this case, the high electrostatic charge of each inserted Mg^{2+} ion is distributed more uniformly among five different Mo_6Se_8 blocks (instead of four). The higher polarizability of the selenium anion, as compared to the sulfur one, ensures the suitable deformation of the anion framework.

Arrangement of the Cation Sites in $MgMo_6T_8$ (T = S, Se) and Its Influence on the Cation Mobility. To understand the reason for the different Mg^{2+} mobilities within the sulfide and selenide hosts, we have to compare the arrangements of the cation sites in the appropriate crystal structures. As was mentioned in the first part of this work,[11] cavity 1 in the rhombohedral $MgMo_6S_8$ is divided into six identical tetrahedra (inner sites; Figure 7a). The minimal distance between two adjacent inner sites is twice as short as that between the closest inner and outer sites: 0.9 and 2.0 Å, respectively. In addition, the outer sites (cavity 2) are less favorable for magnesium occupation because of Mg−Mo repulsion. As a result, the probability for Mg hopping between adjacent inner sites (of the same inner ring) is indeed higher than that between inner and outer sites (inner and outer rings). This leads to a circular motion of the Mg^{2+} ions around the same inner ring. Hence, the Mg^{2+} ions remain confined in a specific cavity 1, rather then migrating to outer sites (in cavity 2) that would eventually allow long-range diffusion in the host's bulk. This is, in fact, the reason for Mg trapping in the crystal structure of $MgMo_6S_8$.

In the triclinic $MgMo_6Se_8$, cavity 1 is divided into two types of sites: two cation-free tetrahedra (CN = 4) and two square pyramids (CN = 5) that can be occupied by cations (Figure 7b). Thus, instead of six equivalent sites in cavity 1, which participate in Mg transport in the sulfides, the selenide possesses only four (two pairs of equivalent sites). It is clear that such an arrangement of the cation sites is not expedient for rhombohedral symmetry. In addition, in contrast to the case of the R CPs, cavities 2 in the T CPs are not structurally, and thus energetically, identical. It should be emphasized that three different types of cavity 2 exist

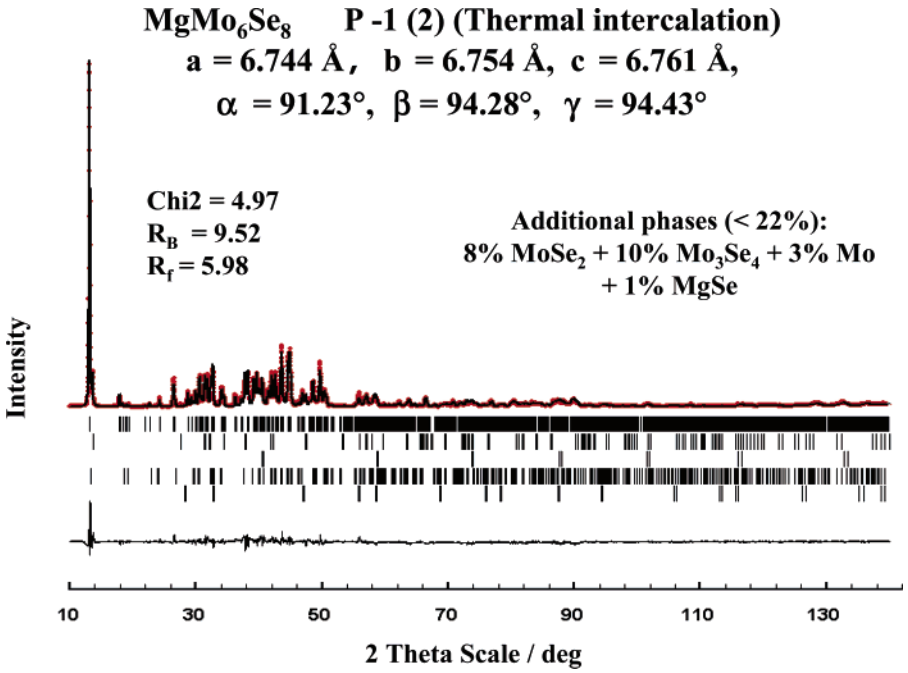

Figure 6. X-ray Rietveld profiles for $MgMo_6Se_8$ obtained by thermal Mg intercalation into Mo_6Se_8.

Table 2. Interatomic Distances (Å) and BVS for Cations in $MgMo_6Se_8$ and $CuMo_6Se_8$

distance	$MgMo_6Se_8$	BV	$Cu_2Mo_6Se_8$	BV
Mo−Mo	2.581(14); 2.651(14); 2.709(13); 2.722(13); 2.762(13); 2.787(13); 3.556(14)		2.680 2.727 3.491	
Mo−Se	2.486(12); 2.495(11); 2.534(12); 2.550(12); 2.563(12); 2.569(11); 2.576(12); 2.580(12); 2.598(13); 2.622(13); 2.631(12); 2.686(12); 2.686(13); 2.687(12); 2.706(12)		2.551 2.565 2.579 2.616 2.673	
Mo−Mg (Cu1)	3.67(2)		3.53	
Mg−Mg (Cu1−Cu1)	1.93(3)		2 × 1.120 2 × 1.940 2.240	
Mg (Cu1)−Se	2.46(2) 2.61(2) 2.64(2) 2.78(2) 2.87(2)	0.685 0.457 0.421 0.288 0.226 ∑ = 2.08	2.464 2.477 2.498 2.501 3.545	0.301 0.291 0.275 0.273 ∑ = 1.14
Se−Se	3.64 3.469/3.833 ± 0.011 the mean value of the 18 shortest distances		3.65 the mean value of the 9 shortest distances	

for all triclinic CPs, but it seems that this fact was not recognized in the literature. As shown below, the diversity of cavities 2 related to the same crystal structure might be a crucial point for the correct analysis of ionic transport phenomena in these hosts.

To carry out such an analysis we have to show the structure of cavity 2 in the polyhedral representation. It is easy to present cavity 2 as a set of linked polyhedra when the latter are occupied by cations, but this is not our case. First, let us take a close look at the structures of cavity 2 known for other CPs. Relatively large ions, like Cr and Mn, occupy the center of these cavities in the CP selenides,[25] but their CN is 6 rather than 8 because of the cavity's distortion. Hence, in this case a pseudo-cubic cavity 2 is divided to one octahedron and two tetrahedra (Figure 8a). For small cations, the anion environment is commonly described as tetrahedral.[1,2,21,25] Thus, pseudo-cubic cavity 2 should be divided into six tetrahedra or three tetrahedra pairs (Figure 8b), where each pair represents two equivalent tetrahedral sites. The latter are connected to each other by the inversion center −1.

In contrast to cavity 1, where the cations can be located in each of the six equivalent tetrahedral sites, only two of the six tetrahedra in cavity 2 are commonly occupied in a given CP. The position of the occupied pair depends on the type of CP: In the first type of CP (with preferential occupation of cavity 1), the linking vector of the pair is approximately parallel to the direction of the channels (close to the direction of the rhombohedral axes), while in the second type of CP, this vector is quasi-normal to the same

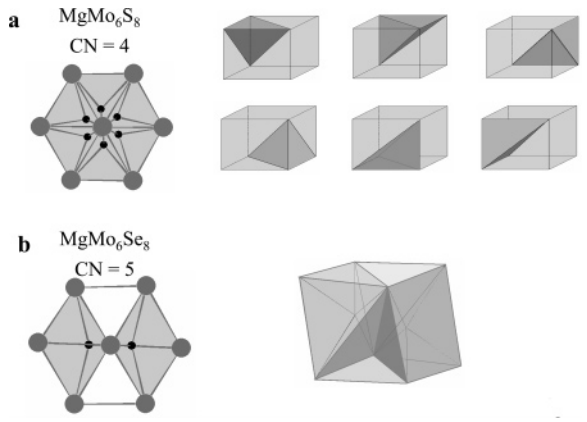

Figure 7. Arrangement of the cation sites in cavity 1 for $MgMo_6S_8$ (a) and $MgMo_6Se_8$ (b). Left-hand side: atomic representation (the projection is normal to the −3 symmetric axis). Right-hand side: polyhedral representation (the polyhedra, which can be occupied by Mg, are darker than the empty ones. Note that for rhombohedral $MgMo_6S_8$, the representation is schematic, and each $[MgSe_4]$ tetrahedron is shown separately).

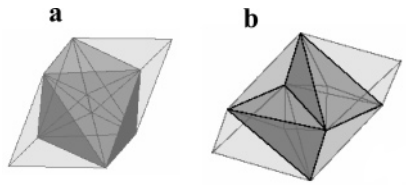

Figure 8. Polyhedral representation of cavities 2 for different CPs: CN = 6 for relatively big cations located in the center of cavity 2 (a); CN = 4 for small cations delocalized from the center of cavity 2 (b).

direction.[21] An exception is found in the crystal structure of one of the sulfoselenides of Ni, where the cations are distributed between two pairs.[20]

These two pairs of the tetrahedra together form the same octahedron known for Cr or Mn. Thus, despite the same total number of tetrahedra in cavities 1 and 2, there is an important difference between their linkages. In cavity 1, all the six tetrahedra have a common edge, which happens to be the shortest diagonal of the cube and lies on a −3 symmetric axis, while in cavity 2, only four tetrahedra are linked by a common edge. Two tetrahedra of the third pair are separated from each other by the octahedron. The occupation of the latter sites by cations is unknown.

According to the Pauling first rule, ionic crystals may be considered as sets of linked polyhedra, while there are only three different options for the linkage of the adjacent polyhedra: common vertexes, common edges, and common faces. Let us apply this rule to our case. Each pseudo-cubic cavity 1 in the CP's crystal structure shares six pseudo-cubic cavities 2. On the basis of the Pauling rule, it is clear that to be linked, the polyhedra in cavities 1 and 2 should make a perfect match. Basically, two different cases for small cations can be regarded. In the case when cavity 1 includes six tetrahedra, every face of the cube is composed of two tetrahedral faces. Thus, to ensure a real linkage between two adjacent cubes (cavity 1 and 2), we have to divide the cavities 2 into six tetrahedra or into a combination of the octahedron and two tetrahedra (Figure 9a).

In contrast, in the case where cavity 1 is a construction of two tetrahedra and two square pyramids, the faces of cavity 1 are not identical: Four of them are divided by the tetrahedra edges, but the two others are the bases of the

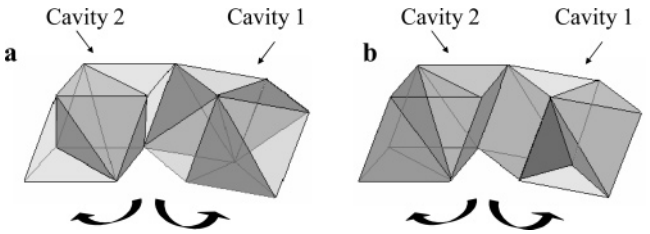

Figure 9. Different linkage correlations between cavities 1 and 2. (a) A sharing cubic face is composed of two triangular faces related to tetrahedra or octahedra. (b) A cubic face is square basic faces of two sharing square pyramids. Note that the cubic cavities are separated for clarity.

square pyramids. As a result, in the latter case, to ensure the linkage by the undivided square faces, the adjacent cavities 2 should acquire the structure either of undivided cubes or of similar combinations of two tetrahedra and two square pyramids (Figure 9b). The latter combination is more realistic in the case of small Mg^{2+} ions.

Thus, to summarize, it can be said that in the crystal structure of triclinic $MgMo_6Se_8$ there are three different types of cavity 2: Two of them include 6 tetrahedral sites, while the third one is composed of two tetrahedra and two square pyramids. This model was taken as the basic one in the search for transport sites in the crystal structure of $MgMo_6Se_8$ (Table 3). The search procedure was similar to the crystal structure refinement. The initial coordinates were those that are known in the literature for different types of CPs or were defined logically from simple geometric considerations. The occupation number for all the sites, except number 1 (that is really occupied), was a minimal one. The refinement was based on soft constraints of "cation−anion" distances in the coordination polyhedra.

The final coordinates of the transport sites, presented in Table 3, were used to calculate the distance of these sites from the Mo and Se atoms (Table 4). According to the latter, it is possible to estimate the validity of the results obtained in Table 3. The ionic radius of the Se atom is equal to 1.93 Å, but as a result of polarization it changes in the CP's crystal structures from 1.80 to 2.08 Å. (See, for instance, the mean value of the nine shortest Se−Se distances[1,2] and the shortest diagonal in cavity 2 for Mo_6Se_8, which are equal to 3.60 and 4.15 Å, respectively.). Thus, in a regular empty tetrahedron of Se atoms, the distance between the Se atoms and the center of the tetrahedra may change from 2.2 to 2.55 Å. As shown in Table 4, the data are very close to these values.

In addition, according to the distances between the sites and molybdenum atoms "M−Mo", it is clear that only classic inner and outer sites in the crystal structure of $MgMo_6Se_8$ can be occupied by cations at ambient temperature. Other sites can serve only as transport sites because they are too close to the Mo atoms. Their distances from the Mo atoms are indeed shorter than the sum of the metallic radii of Mg (1.60 Å) and Mo (1.39 Å), equal to 2.99 Å. However, as mentioned previously, the positions of these sites in the crystal structure provide an understanding of the peculiarities of the cation motion in the CPs.

In fact, according to the data collected in Table 3, we can construct a map for all the cation sites in the crystal structure of $MgMo_6Se_8$ (Figure 10) and choose the most favorable

Table 3. Coordinates of All the Cation Transport Sites in the $MgMo_6Se_8$ Crystal Structure.

site number	cavity	site position	*X*	*Y*	*Z*	CN	additional information	ref
1	1	2i	0.116(3)	0.925(3)	0.999(3)	5	shift from the inner sites	1
2	1	2i	0.034(3)	0.067(3)	0.898(3)	4	shift from the inner sites	1
3	2-1	2i	0.015(7)	0.368(10)	0.949(6)	4	shift from the outer site	1
4	2-1	2i	0.939(3)	0.490(3)	0.894(3)	4	"new cation location"	21
5	2-1	2i	0.882(3)	0.710(3)	0.116(3)	4	geometric considerations	
6	2-2	2i	0.955(3)	0.033(3)	0.374(4)	4	shift from the outer site	1
7	2-2	2i	0.900(3)	0.941(3)	0.504(3)	4	"new cation location"	21
8	2-2	2i	0.109(7)	0.872(7)	0.697(7)	4	geometric considerations	
9	2-3	2i	0.305(9)	0.920(6)	0.059(7)	5	shift from the outer site	1
10	2-3	2i	0.508(7)	0.875(7)	0.927(7)	4	"new cation location"	21

Table 4. Interatomic Distances (Å) and BVS for All the Cation Sites in $MgMo_6Se_8$

			distance						distance		
cavity	site	CN	M−Mo	M−Se	BV	cavity	site	CN	M−Mo	M−Se	BV
1	M1	5		2.46(2)	0.685	2-2	M6	4		2.41(2)	0.784
			3.66(2)	2.61(2)	0.457				3.17(2)	2.41(2)	0.784
			3.91(2)	2.64(2)	0.421				3.17(2)	2.41(2)	0.784
			4.25(2)	2.78(2)	0.288				3.24(2)	2.41(3)	0.784
				2.87(2)	0.226				4.04(2)		$\Sigma = 3.12$
					$\Sigma = 2.08$		M7	4	2.46(2)	2.35(2)	0.922
	M2	4		2.52(2)	0.582				3.20(2)	2.35(2)	0.922
			3.66(2)	2.53(2)	0.567				3.21(2)	2.38(2)	0.850
			4.17(2)	2.54(2)	0.552				3.73(2)	2.38(2)	0.850
			4.24(2)	2.54(2)	0.552						$\Sigma = 3.54$
					$\Sigma = 2.25$		M8	4	2.63(5)	2.32(5)	1.000
2-1	M3	4	3.14(5)	2.39(4)	0.828				3.19(5)	2.32(5)	1.000
			3.28(4)	2.39(5)	0.828				3.50(5)	2.36(5)	0.898
			3.32(5)	2.39(5)	0.828				3.85(5)	2.37(5)	0.874
			3.97(5)	2.39(6)	0.828						$\Sigma = 3.77$
					$\Sigma = 3.31$	2−3	M9	5		2.44(4)	0.723
	M4	4	2.45(2)	2.33(2)	0.973				2.91(5)	2.44(5)	0.723
			3.17(2)	2.33(2)	0.973				3.37(5)	2.53(6)	0.567
			3.33(2)	2.34(2)	0.947				3.58(5)	2.58(5)	0.495
			3.78(2)	2.34(2)	0.947				3.78(5)	2.80(5)	0.273
					$\Sigma = 3.84$						$\Sigma = 2.78$
	M5	4	2.66(2)	2.31(2)	1.027		M10	4	2.39(5)	2.31(5)	1.027
			3.35(2)	2.32(2)	1.000				3.13(5)	2.31(5)	1.027
			3.44(2)	2.34(2)	0.947				3.15(5)	2.33(5)	0.973
			3.84(2)	2.37(2)	0.874				4.00(5)	2.33(5)	0.973
					$\Sigma = 3.85$						$\Sigma = 4.00$

route for Mg^{2+} ion transport. In such an analysis, we should take into account (i) the distance between the adjacent cation sites, (ii) the distance between the sites and the Mo atoms, and (iii) the size of anion polyhedra around the sites and their linkage. As discussed previously, the smaller the polyhedron formed by the anions, the higher the BVS or the positive charge of the cation located in the center of this polyhedron. Hence, Table 4 also presents the BVS calculated according to eqs 3 and 4: The distances between each site and the centers of the neighboring selenium atoms were taken as the lengths of the chemical bonds for an imaginary cation located at this site. Note that there is a clear correlation between the BVS values and the distances of the sites from the Mo atom; the higher the BVS, the closer the site to the Mo atom. A similar method of BVS mapping is known as a valuable tool for cation location and transport examinations.[27]

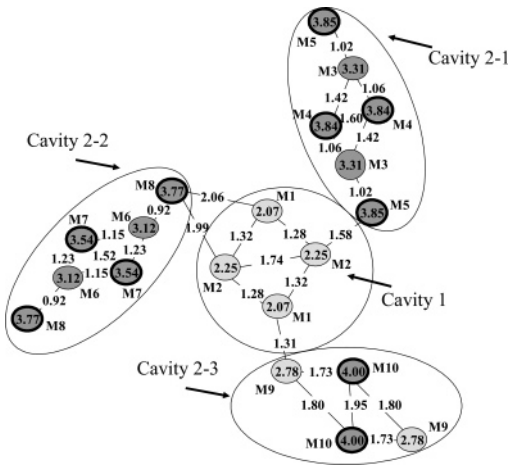

Figure 10. Map of the cation sites in the crystal structure of $MgMo_6Se_8$.

Thus, the circles in Figure 10 represent the cation sites in the CP's crystal structure, while the values inside these circles are the BVS values for these sites. Sites that are too close to Mo are marked by a thick circuit line. One can see that the tetrahedral sites in cavities 2-1 and 2-2, as well as the M10 sites in cavity 2-3 (dark colored circles), are less suitable for the Mg^{2+} ion transport than the sites in cavity 1 and the M9 sites in cavity 2-3 (light colored circles) as a result of their small size. In addition, the distance of 1.28−1.32 Å between the inner sites (M1 and M2), is very close to that of 1.31 Å between the inner and the outer sites (M1 and M9). Moreover, the coordination polyhedra around the latter sites are square pyramids sharing their bases, while a common face of the tetrahedron around M2 and the pyramid around M1 has a triangular shape. It is clear that the hopping through the square anion arrangement is essentially easier than that through the triangular one. Thus, the activation energy of the hopping between inner and outer sites might

be even lower than that between inner sites. This low activation energy results in the absence of Mg trapping, as well as in high Mg mobility in the triclinic $MgMo_6Se_8$.

Conclusions

Mg insertion into rhombohedral Mo_6Se_8 results in the formation of the triclinic phases $Mg_xMo_6Se_8$ ($x = 1$ and 2). Rietveld refinement of powder XRD and neutron diffraction profiles was used to solve the crystal structure of $MgMo_6Se_8$: space group $P\bar{1}$, $a = 6.743$ Å, $b = 6.755$ Å, $c = 6.761$ Å, $\alpha = 91.22°$, $\beta = 94.29°$, and $\gamma = 94.44°$. According to the position of the Mg^{2+} cations, this compound may be related to the classic triclinic CPs with statistic occupation of two identical sites in cavity 1 (so-called dumbbells). The anion environment of the Mg^{2+} cations is square pyramid (CN = 5). Thus, the crystal structure is similar to that of $Fe_2Mo_6S_8$.

An analysis of all the coordination polyhedra, including the cation-free sites (transport sites), showed that cavity 1 in the crystal structure of $MgMo_6Se_8$ is composed of two square pyramids and two tetrahedra, in contrast to the $Mg_xMo_6S_8$ sulfides ($x = 1$ and 2) with six identical tetrahedral sites in cavity 1. In addition, there are three different types of cavity 2 in the CPs under study: Two of them include six tetrahedral sites, while the third one is composed of two tetrahedra and two square pyramids. On the basis of this polyhedral model, the positions of all the transport sites were refined. The latter allow the identification of the routes in the crystal structure, which are favorable for the transport of the Mg^{2+} ions.

As shown in the first part of our work devoted to sulfides, the ring arrangement of the six cation sites with low occupation energy (inner sites in cavity 1) results in a circular motion of the Mg^{2+} ions between these sites, instead of a progressive diffusion to the bulk (The latter necessitates hopping between inner and outer sites in cavity 2). This leads to Mg trapping in the crystal structure of $MgMo_6S_8$. In contrast, according to the arrangement of the cation sites in triclinic $MgMo_6Se_8$, the hopping between the inner and the outer sites should be even more favorable than that between inner sites. This results in the absence of Mg trapping and, accordingly, in high Mg mobility in the latter compound. Thus, the comparative analysis of the Mg transport routes within the crystal structure of the sulfides and selenide allows an understanding of the peculiarities of their different electrochemical behaviors.

Acknowledgment. Partial support for this work was obtained from the Israel-US binational foundation (BSF). The Institut Laue Langevin is warmly acknowledged for providing the neutron facilities.

Supporting Information Available: Crystallographic information in the form of a cif file. This material is available free of charge via the Internet at http://pubs.acs.org.

CM060715M